TITLE: **SPIRE Test Facility: optical tests & characterisation report**

By: Marc Ferlet (RAL)

DISTRIBUTION

- RAL/SSTD - SPIRE Project Team:
  For info:
  - B Swinyard (RAL)
  - D Smith (RAL)
  - T Lim (RAL)
  - E Sawyer (RAL)
  - D Griffin (RAL)

  For Project database/archive:
  - J Long (RAL)

CHANGE RECORD

ISSUE	DATE	SECTION	REASON FOR CHANGE
1.0	04/05/04	All	First issue of the document
1.1	10/05/04	5 & Annex	Update of results
2.0	09/01/06	All	Extension of mode decomp, addition of TFTS and Photomixing source sections

CONTENTS

APPLICABLE AND REFERENCE DOCUMENTS

RD1 SPIRE-RAL-NOT-000621v4
RD2 SPIRE-RAL-NOT-000622v3
RD3 SPIRE RAL-NOT-000734v2
RD4 SPIRE-RAL-NOT-001258v1
RD5 SPIRE calibration lab / Laser log-book

1. INTRODUCTION

This note summarises a series of experiments performed with the different optical subsystems and related sources (FIR laser, TFTS & HBB, Photomixing source) in the SPIRE calibration lab over the last few months and years.
Although several notes have been circulated around within the Project and have been already included in log book, it was found useful to compile in a single TN the results of these tests concerning the SPIRE ground-calibration sources and related optical instrumentation.
Results of FIR beam characterisation from different set of measurements are reported in section 2. Section 3 deals with the broadband and spectrally modulated source (HBB feeding the Test facility Fourier Transform Spectrometer). And finally, some notes on the photomixing source, recent addition to the possible calibration sources are given in section 4.

2. FIR LASER

2.1 Brief description of the optical systems

The optical instrumentation used in the different test is illustrated in the pictures below. The 2 pictures focus on the present instrumentation on the 2 main optical benches outside the cryostat. Details of the design and implementation, component and system particularly for the Telescope Simulator, are given in RD1-4.
Only section 4 & 5 are using partially or completely the instrumentation shown below. Simplified test configuration for FIR laser only characterisation is described along side the results in section 3.
Although the optical systems on the separate benches are protected by enclosures which can be purged with dry air to limit the effect of atmospheric absorption over a max optical path (outside cryostat) estimated to ~6m, none of the tests in the following section used the purge system (i.e. propagation in air).

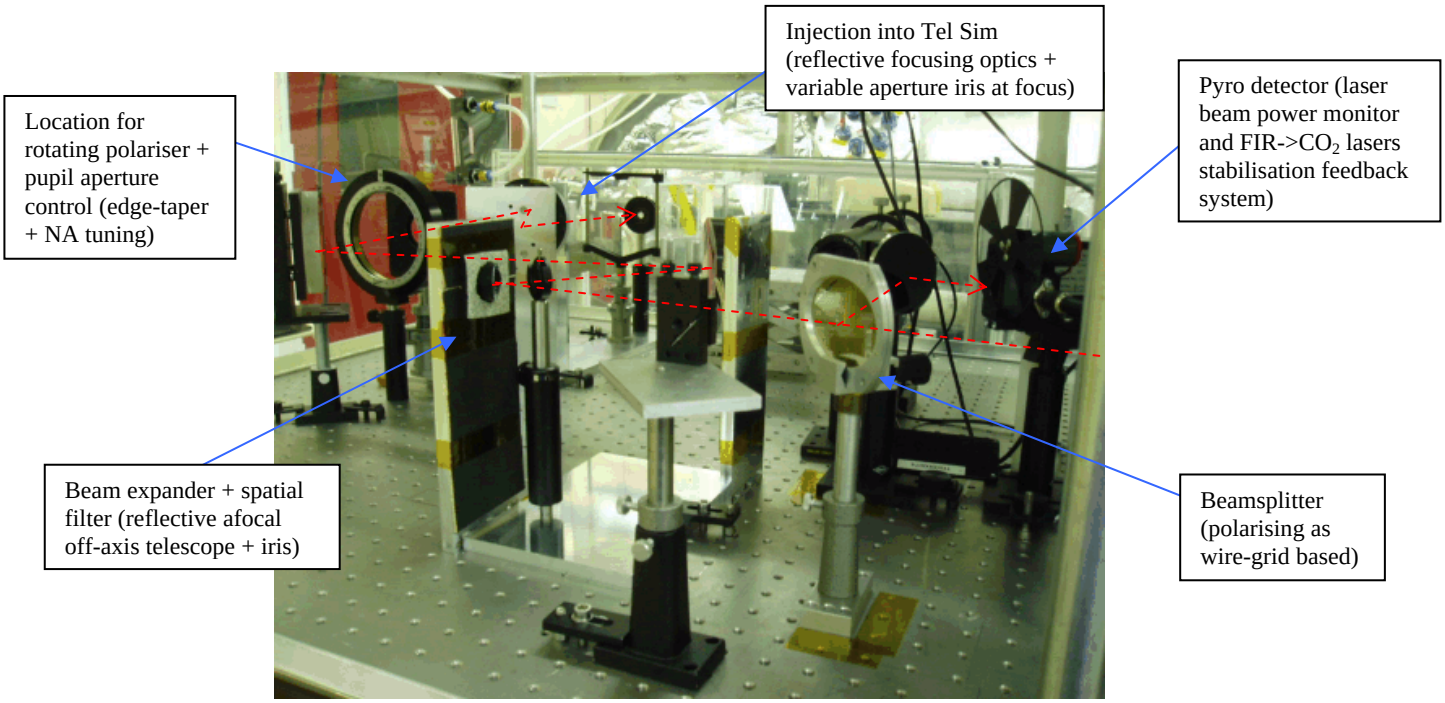

Figure 1: FIR laser bench set-up (05/05/2004). The FIR laser beam path from the FIR cavity output window (+ 100cm^{-1} long pass edge filter) is outlines in red (dashed line). Extra alignment components such as HeNe laser + beam expander + mirror are also present.

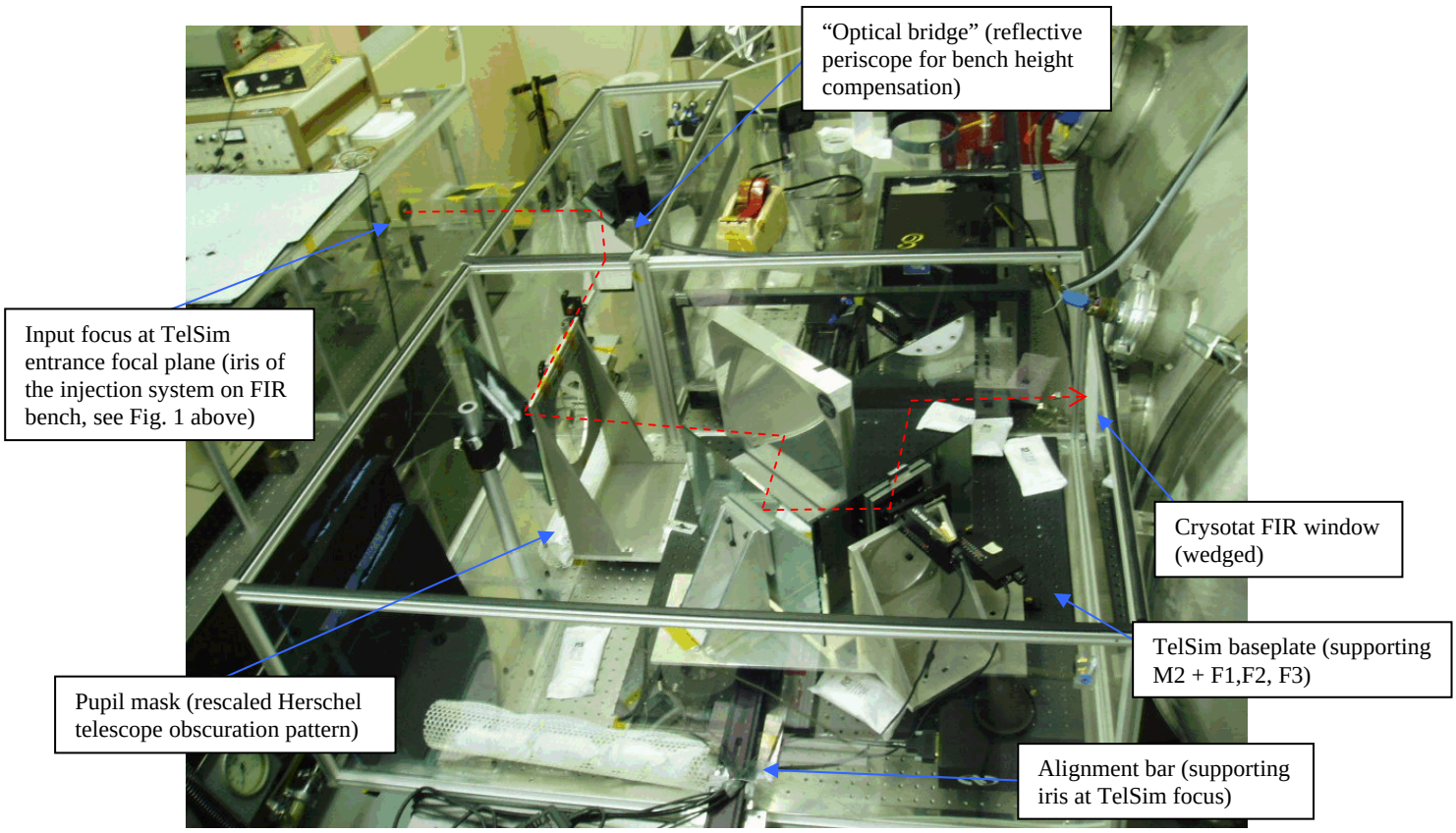

Figure 2: Telescope Simulator main bench (05/05/2004). The FIR laser beam path from the FIR bench output to the calibration cryostat optical port (FIR window) is outlines in red (dashed line).

2.2 FIR laser output beam test & characterisation

Report on the FIR laser beam characterisation. Test performed in SPIRE cryolab on 30/09/03.

FIR output wavelength: 214μm, linear vertical polarisation (verified with rotated wire grid)

FIR beam total power: ~2mW max at cavity output

Optics: Off-axis (60°) single paraboloid, Al protected (Janos Tech), f_{eff}=152.4mm, located ~900mm from laser cavity output plane

Detector (at optics focus): Spiricon/PYROCAM III, room-temperature pyroelectric 124x124 detector array, pixel size~100μm (demo. on-site by UK distributor)

Remarks: FIR beam considered as stable enough, no use of the stabilisation feedback system; manual alignment of camera wrt beam focus.

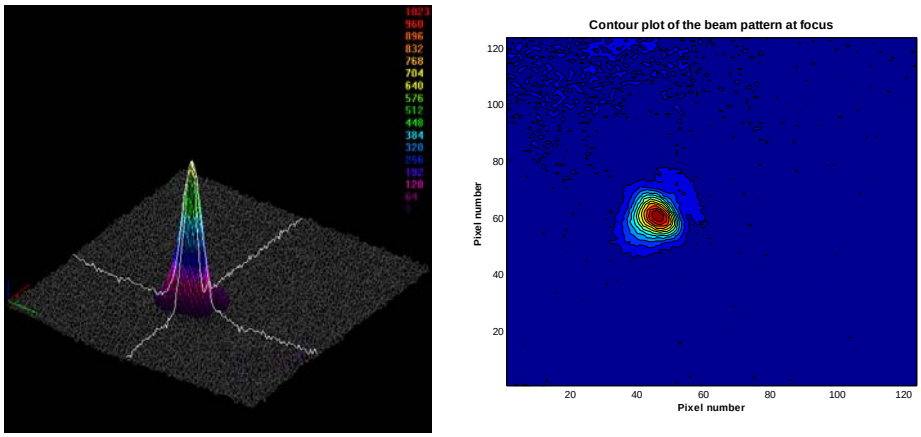

Figure 3: Beam pattern (3D intensity view and contour plot) of the focused FIR laser beam at 214μm after acquisition by PYROCAM III camera system. Summation and averaging were used to improve SNR.

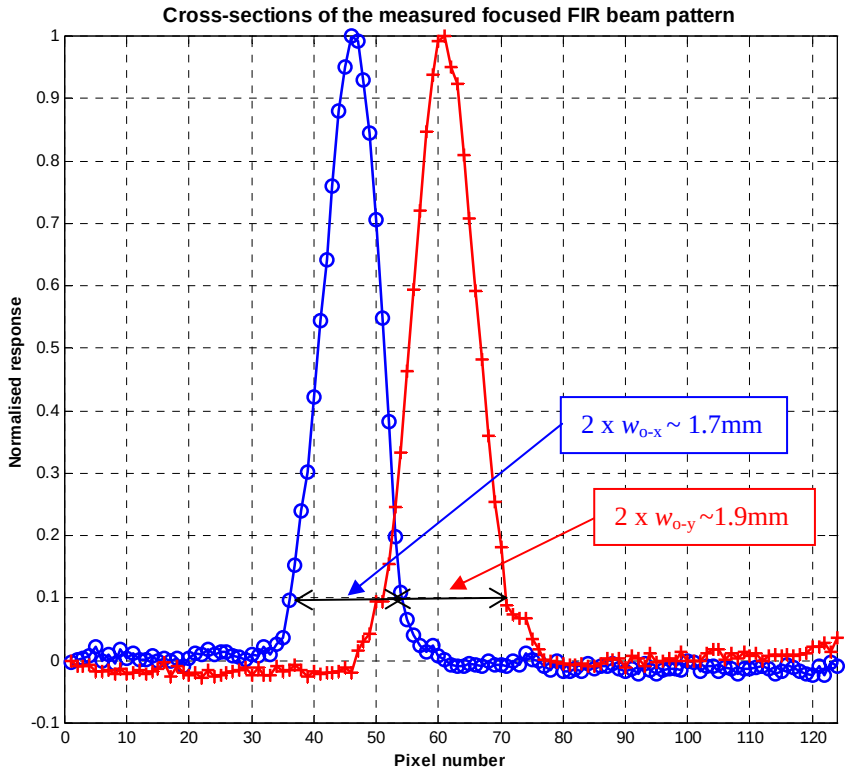

The above values for the waist were obtained by fitting a FMGB to the normalised data for the 2 main planes (see below). The average value for the waist is w_o=0.9±0.1mm when a FMGB is assumed. The ~10-15% uncertainty arises from the sampling at detector as well as some potential residual astigmatism and coma from angular misalignment in (manual) camera positioning.

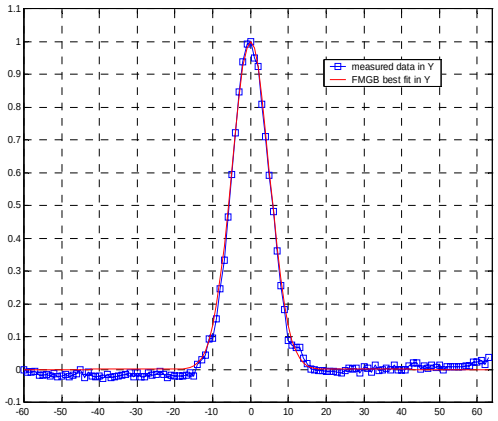

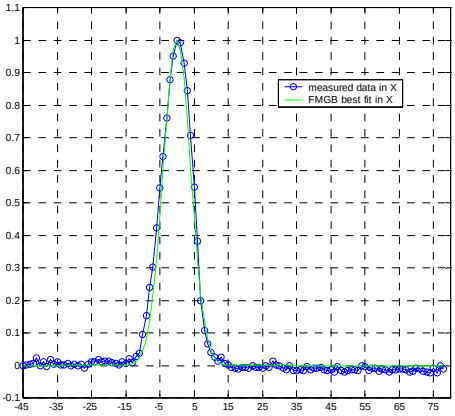

Under the same assumption that the FIR cavity is delivering a FMGB, we can in parallel estimate the expected wait size at mirror focus. The test configuration (different from figure 2) is summarised by the sketch below.

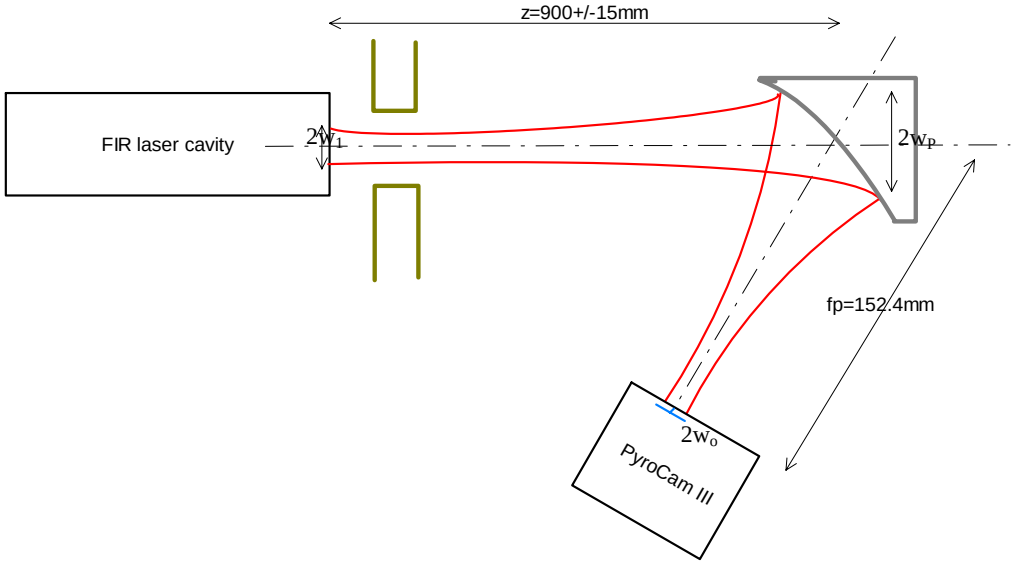

The laser starts with an initial waist w_1=6.0±0.5mm at the output of the FIR cavity. The free-space propagation of the assumed single mode GB up to the paraboloid mirror gives rise to a $1/e^2$ beam radius w_p on the mirror given by:

$$> \quad wp := w1\sqrt{1+\left(\frac{\lambda\, z}{\pi\, w1^2}\right)^2}$$

Its value is w_p=11.85mm at λ=214μm. We can check at this point that the mirror is well oversized (aperture diameter is 76.2mm) compared to the beam so that no noticeable additive diffraction effect from (low) illuminated mirror edge is to be expected here. The parabolic mirror refocuses the beam and the new waist w_o assumed to be located close to geometric focus (not probed in the experiment) and where the camera is located is given by:

$$> \quad wo := \frac{fp\,\lambda}{\pi\, wp}$$

One can also consider the angular aperture approach which gives $w_o=(2/\pi)F\lambda$ where the focal ratio for $1/e^2$ is given by $F=f_p/(2w_p)$. As F~6.4 here, the focused beam is slow enough for the paraxial approximation to apply and both formulas lead to w_o=0.88mm.
Uncertainty on this value results from the addition (error assumed independent) of the ~2% relative uncertainty on the distance z and the ~8% uncertainty on the initial waist size w_1. The final theoretical estimation of the expected waist size for a FMGB FIR line in this configuration is w_o=0.88mm±10%. This agrees well with the above measurement and allows concluding that, at first order (under FMGB approximation) the FIR laser line at 214µm delivers a coherent single mode Gaussian beam.

2.3 FIR laser beam measurement at TelSim focus

Test performed in SPIRE cryolab on 16/12/03 with Golay cell (+ chopper) at the TelSim focus located at the end of the alignment bar (see Fig 2; F1 removed, direct path from M2 to detector at focus). Details of the FIR laser status and experimental conditions are given in RD5.

NB: The experiment was carried out after the replacement of the FIR laser Brewster window (ZnSe plate) at the entrance of the FIR laser cavity.

Beam size only measurements performed at 2 different wavelengths:

- 214µm (FIR gas = DFM) for comparison with above measurements,
- 392µm (FIR gas = MA) for longer wavelength effect assessment (e.g. increase in diffraction).

Modelling of the expected beam pattern and comparison with experimentally measured beam size along vertical axis is given below.

Convolution of Gaussian function => application to finite aperture detector effect (e.g. the Golay cell entrance aperture) on single mode Gaussian Beam detection.

```
> restart;func_f:=x->(exp(-x^2/wo^2))^2;
```

$$func\_f := x \rightarrow \left(\mathbf{e}^{\left(-\frac{x^2}{wo^2} \right)} \right)^2$$

```
> convol:=int(func_f(x-t),t=(-L/2)..(L/2));
```

$$convol := -\frac{1}{4}\sqrt{\pi}\,\sqrt{2}\,wo\,\mathrm{erf}\left(\frac{\sqrt{2}\,(-L+2x)}{2\,wo}\right) + \frac{1}{4}\sqrt{\pi}\,\sqrt{2}\,wo\,\mathrm{erf}\left(\frac{\sqrt{2}\,(L+2x)}{2\,wo}\right)$$

At TelSim input focus (FIR bench: output of the injection system, see Fig 1) at 214µm:

```
>L:=3.5;lambda:=0.214;F_number:=8;wo:=evalf((2/Pi)*F_number*lambda);plot(convol/maximize(convol,x=-5..5),x=-4..4);
```

$$L := 3$$

$$\lambda := 0.214$$

$$F\_number := 8$$

$$wo := 1.089893050$$

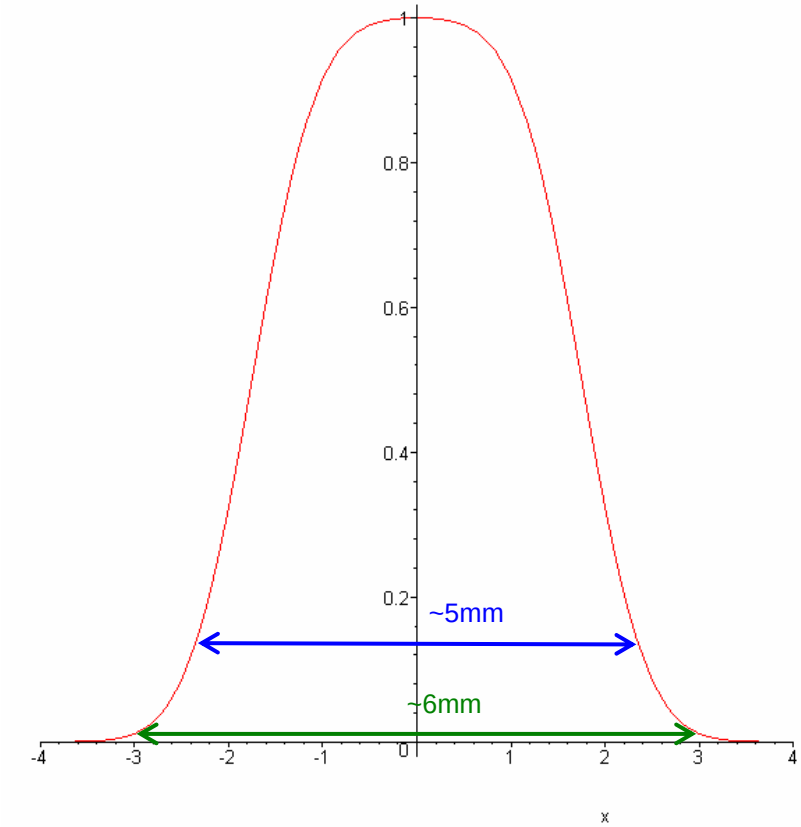

The blue arrow range is the estimate of the $1/e^2$ beam diameter from measurement and the green arrow range is the estimated full beam diameter from measurement at the limit of detection (limited by background noise + detector noise, absorption through long path) with the Golay cell. Agreement with the model is good, including the more flat-top central shape as expected (although difficult to characterize precisely due to measurement uncertainty linked to laser output stability).

At TelSim final focus (see Fig. 2; F1 removed), same detector (Golay cell), at 392µm:

```
>L:=4.0;lambda:=0.392;F_number:=8.7;wo:=evalf((2/Pi)*F_number*lambda);plot(convol/maximize(convol,x=-5..5),x=-6..6);
```

$$L := 4.0$$

$$\lambda := 0.392$$

$$F\_number := 8.7$$

$$wo := 2.171128071$$

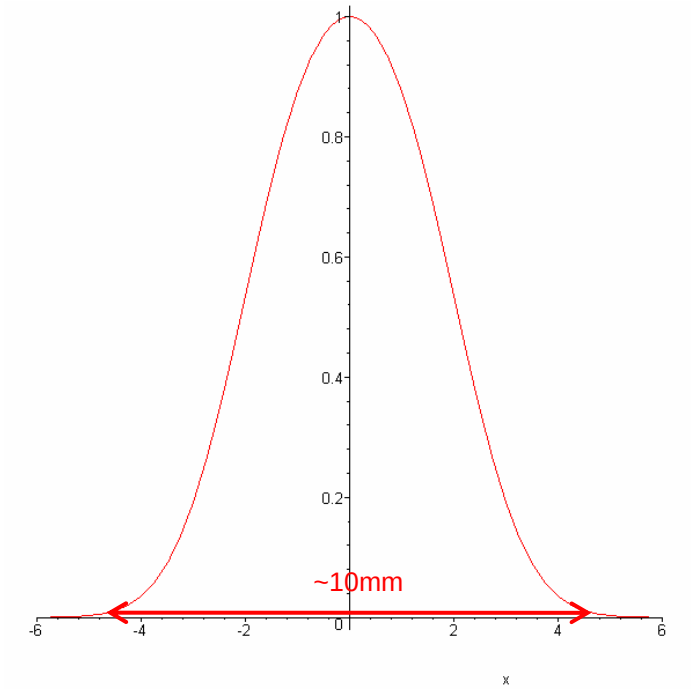

Full beam diameter estimate by measurement is show in red arrow range. The level of detection may be higher than shown above but the edge-taper at pupil mask will increase by 5-10% the waist at focus so the agreement appears good also at long wavelength.

NB: fluctuations of 15-20% minimum in average on the measured signal were recorded during the tests.

2.4 FIR laser beam measurement at TelSim focus inside Calibration cryostat

This series of tests was performed on 22 and 23/04/04 and used the complete path, as described in section 2, from FIR laser cavity to focal plane inside calibration cryostat (ultimately confocal with the entrance focal plane of SPIRE during ground-testing).
The tests were performed after the 1st series of SPIRE CQM performance tests. Some of these tests used the FIR laser at 432µm (FIR gas =FA; see RD5) i.e. the centre of SPIRE PLW band. The full PLW focal plane array response to point source illumination with the laser was not expected. Although laser illumination of the array might have been far above the detection range of SPIRE, it was found necessary to assess if the point source laser illumination issue is not coming from instrumental effect outside SPIRE itself (i.e. bulk and/or surface scattering from cryostat window, speckle from coherence effect after multiple reflections within tilted cryostat filter, …). The results discussed in section 4 demonstrates that the TelSim is focussing well the injected laser beam into a GB pattern focal plane irradiance in good agreement with expected diffraction-limited beam shape from theory.

The specific detection system located temporary inside the cryostat is shown in the picture below.

Attenuation of the beam was found to be needed and performed via insertion of paper in the collimated section of the beam path on the FIR bench. Calibration of the paper showed an attenuation of ~1.05±0.10dB/sheet, very reproducible and consistent with same data obtained during SPIRE CQM test campaign at he same wavelength.

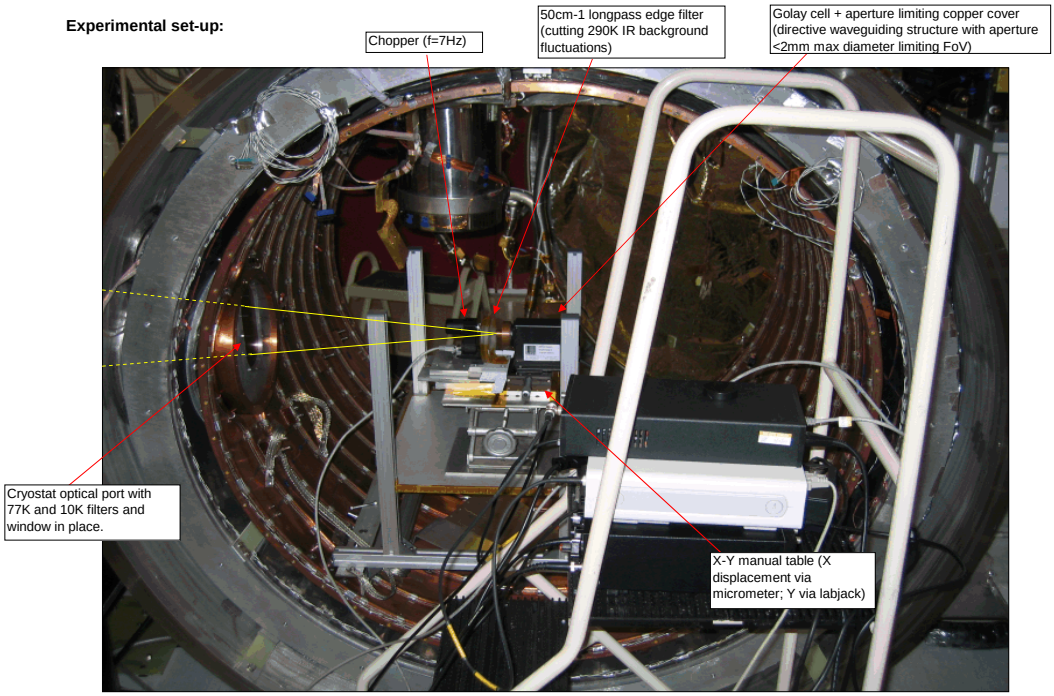

Figure 4: Details of the experimental detection system used for laser beam profile measurement inside cryostat.

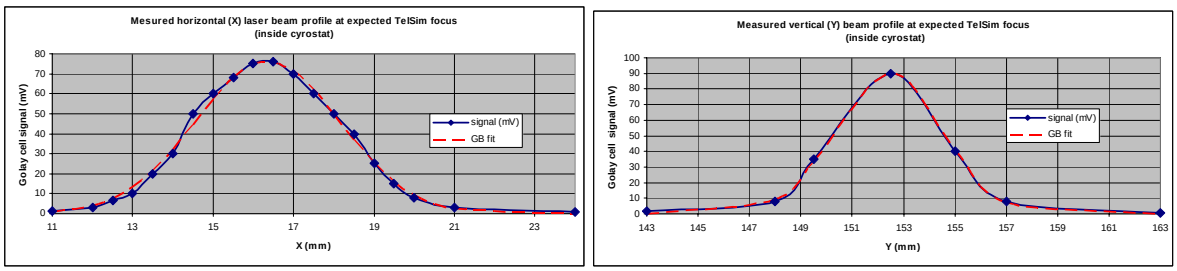

Figure 5: Measured (and fits) transverse laser beam profiles at best focus inside cryostat

Using the TelSim multi-axes control, defocus was induced via displacement of the Trombone formed by the combination of flat mirrors F1+F2. Then 2 other transverse profiles were manually recorded. The laser output was found very stable during the each data recording period.

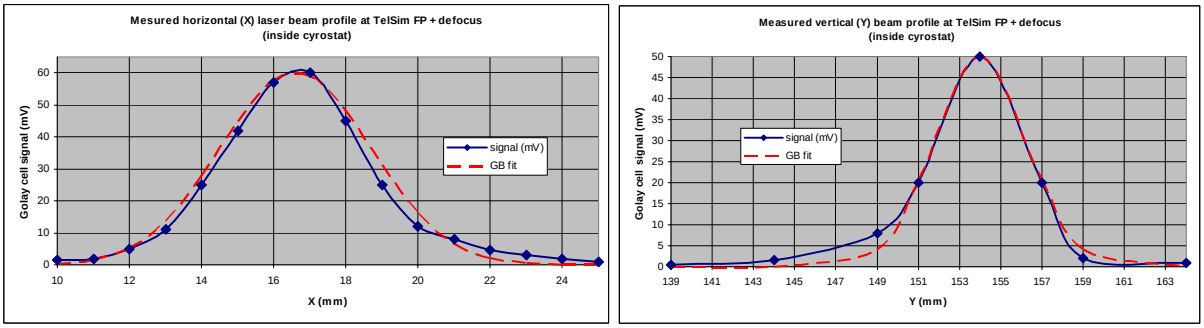

Figure 6: idem at figure 5 but with 30mm defocus on TelSim.

NB: The laser output showed fluctuations of ~5% in the best focus case and ~11% in magnitude during the defocus beam probing.

From the fitted (GB spatial model) experimental data, the following measured beam characteristic parameters (waist size at best focus and beam radius at defocus position) at 432µm were derived:

F= 8.68 **wo theo=** **2.48** mm for reference **~4.5** **dB edge taper**

	wo x (mm)	FWHMo x (arcsec)	wz x (mm)	FWHMz x (arcsec)
Best fits in x:	3.56	30.42	4.17	35.58
	wo y (mm)	**FWHMo y (arcsec)**	**wz y (mm)**	**FWHMz y (arcsec)**
Best fits in y:	4.12	35.03	4.48	38.15
Averages=	3.84	32.72	4.325	36.86

The (Herschel-)equivalent FWHM on sky are given as indications. Applying FMGB propagation law, the defocus value in x and y are well-explained (within ~2-3% deviation) for a 60mm defocus from best focal plane which corresponds to the TelSim defocus setting of 30mm (half of the effective displacement). Difference in beam size in x and y may come from the relative lack of precision on the y measurement (labjack vertical displacement compared to micrometer control in x). Residual TelSim astigmatism along side beam polarisation could also contribute (TBI) to the slight elliptical shape, elongated along y (i.e. the SPIRE Phot long length direction).

It was also checked that for the above derived parameters (see attached spreadsheet "***SPIRE_FIRlaser+TelSim characterisation_UPDATED.xls***"), the closest GSM (=Gaussian Shell Model) is well within the paraxial approximation of the spatial-spectral domain.

2.4.1 Through-focus

By varying the TelSim trombone position, a through-focus probing of the peak beam irradiance at different out-of-focus planes was performed. For each defocus, position compensation with TelSim scan angular control (2-axes, on F2 and F3) was made.

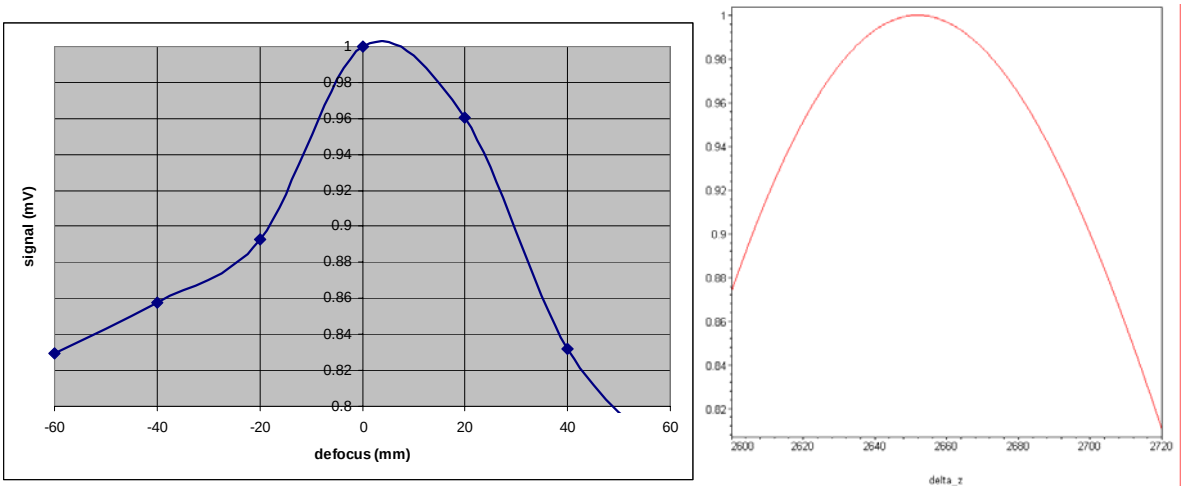

Figure 7: Normalised beam peak irradiance: as-measured (left) and as-modelled (right).

The measurements are compared to simulation from a model based on diffracted truncated GB with an axial irradiance given (before normalisation) by the following closed-form expression:

$$Iaxial := z \rightarrow \frac{2\,\pi\,a^2\,T^2\left(\coth\left(\frac{1}{T^2}\right)-\frac{\cos\left(\frac{\pi\,N\,(R-z)}{z}\right)}{\sinh\left(\frac{1}{T^2}\right)}\right)}{\lambda^2\,z^2\left(1+\frac{\pi^2\,T^4\,N^2\,(R-z)^2}{z^2}\right)}$$

where a is the radius of the Herschel exit pupil (virtual simulated), T is the truncation parameter set to represent the estimated ~4.5dB edge-taper from the experiment, R is the distance from simulated exit pupil to best geometric focus and N is the Fresnel number (here ~20). From Figure 7 above, one can see that qualitative agreement is found, although deeper interpretation would be difficult due to estimated ~20% relative uncertainty on the measurements (laser fluctuations + reset during the measurement campaign; angular misalignment of the detector with fixed pointing during through-focus scan wrt to TelSim beam). Nevertheless the axial region over which the Strehl ratio is > 85% is in agreement with the depth of focus (approx. the Rayleigh range).

2.4.2 Modal decomposition

Based on the assumption that the detected beam could be a general partially coherent beam of GSM type formed by independent superposition of Hermite-Gauss modes, a modal structure decomposition, see below, has been performed on the fitted data (averaged value at best focus):

$$I_{fitted\ data}(x)=\sum_{n=0}^{\infty}c_n.\left(HG_n(x)\right)^2 \quad \text{with} \quad HG_n(x)=\left(\frac{2}{\pi\,\omega_o}\right)^{1/4}.\frac{1}{\sqrt{2^n n!}}.H_n\left(\frac{x\sqrt{2}}{\omega_o}\right).e^{-\frac{x^2}{\omega_o^2}}$$

$$\text{and} \quad c_n=2\pi^2\,\omega_o^2\int_0^{\infty}FT\left[I_{fitted\ data}(x)\right](u).\Psi_n(\pi^2\,\omega_o^2\,u^2).u.du \quad \text{with} \quad \Psi_n(t)=L_n(t).e^{-t/2}$$

where H_n and L_n are the n^{th}-order Hermite and Laguerre polynomials respectively.

The modal decomposition is first performed with a free-space (not diffracted) GB at focus of a similar. By definition this reference beam is single-moded. The decomposition of the measured beam at focus wrt the free GB beam with waist given by $w_o=(2/\pi).F.\lambda$ (with F~8.7 in the experimental set-up).

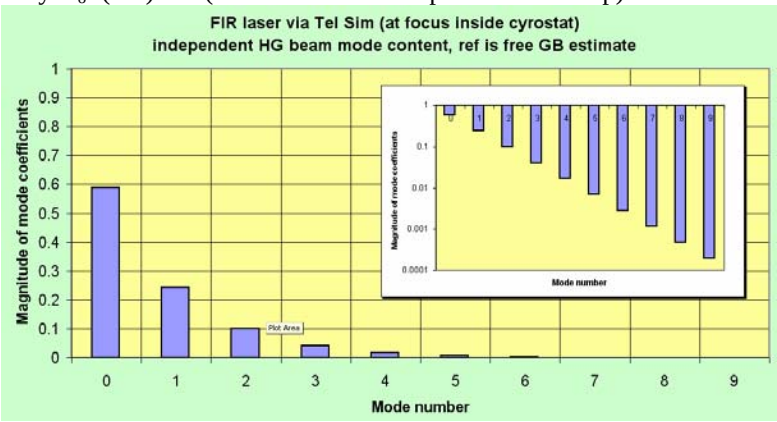

The measured beam can be then globally characterised by the beam propagation factor M^2 which is retrieved from the coef of the decomposition. Only the relative proportion of single-mode GB left is only 58%.

			error
Mode contents	**c0**	0.588668	5.0%
	c1	0.242138	-7.2%
	c2	9.96E-02	-19.4%
	c3	4.10E-02	-31.5%
	c4	1.69E-02	-43.7%
	c5	6.93E-03	-55.9%
	c6	2.85E-03	-68.1%
	c7	1.17E-03	-80.3%
	c8	4.82E-04	-92.4%
	c9	1.98E-04	-104.6%
Sum should be equal to 1:		*0.999861*	
	M^2	***2.39***	7.0%

It is interesting to change reference for the decomposition and use this time a clipped (diffracted; with edge-taper corresponding to experimental set-up i.e. estimated to 4.5dB at TelSim pupil edge) GB beam focused with same F#. The beam obtained at best focused is then characterised by a waist[1] w_{diff}=3.23mm.

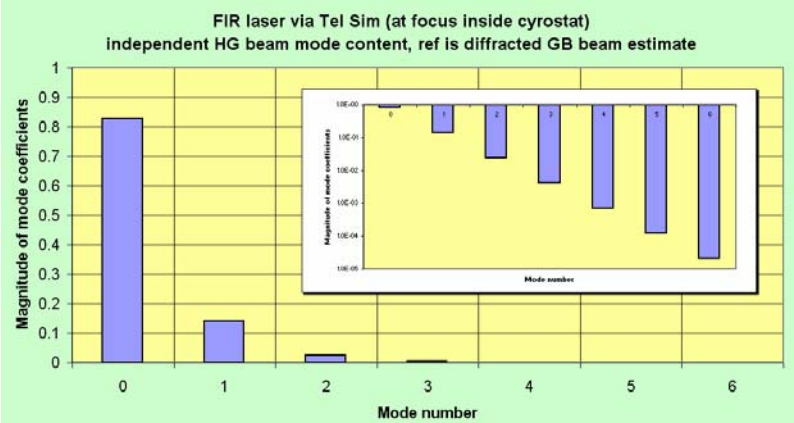

The respective mode content is given in the table below indicating a low fractional amount of higher order-mode with a relative M2 factor now close to 1.4. This indicates that the measured end-to-end beam delivered by the TelSim at this wavelength (432μm) is close to a perfectly diffracted GB beam.

			error
Mode contents	**c0**	0.828715	5.0%
	c1	0.141946	-24.3%
	c2	2.43E-02	-53.5%
	c3	4.16E-03	-82.8%
	c4	7.13E-04	-112.0%
	c5	1.22E-04	-141.3%
	c6	2.09E-05	-170.6%
Sum should be equal to 1:		*0.999996*	
	M^2	***1.41***	9.3%

The residual contribution to the M^2~1.4 (i.e. presence of residual modes of order 1 and 2) is qualitatively explained by possible further diffraction at aperture edges along the path (i.e. not at the pupil like for cryostat filter apertures) as well as source transverse coherence issue (phase and amplitude fluctuations of laser on different time-scale and spectral degree of coherence clipping before injection into TelSim) and end-to-end optical chain residual aberrations.

Back on the previous case: the difference seen in the values of the M^2 factor (~2.4 compared to 1) when comparing the measured beam with a freely propagated GB is explained by dominant contribution of diffraction, as expected from relatively high pupil edge illumination, inducing the scattering of the initial reference single-mode GB into higher-order modes

NB: Error in the mode coefficient increases exponentially: assuming ~5% on C_0, it becomes ~51% on C_1, ~107% on C_2 and so on… But the insert in the above figure shows the rapid (actually exponential) decreases of the mode coefficients so that large errors on higher order have no impact on the main interpretation. A weighted error estimates for the derived M2 is also given.

[1] Numerically computed via H.Urey approach in Applied Optics vol43 no3 (January 2004). It should be noticed that the FHWM of the diffracted beam is computed by same approach to $FWHM_{diff}$=4.03mm while a derived value of the FHWM from the computed diff GB waist will give $FWHM_{derived}$=sqrt(2.ln(2)).w_{diff} =3.80mm indicating that the diff GB is as expected spatially broader than a pure single-mode GB rescaled for the computed waist.

3. TEST FACILITY FOURIER TRANSFORM SPECTROMETER (TFTS)

3.1 TFTS requirements: optical interface to existing/designed AIV hardware

Here is a list, released initially 20/09/02, of the general specifications and interface constraints for an AIV FTS. In order to perform on-ground calibration of the Herschel-SPIRE instrument, different calibration sources are needed. Among them, an FTS, external to the calibration cryostat, is desirable for calibration of SPIRE photometer and spectrometer spectral responses. The remarks below should help defining the interface of this AIV FTS with the present design of the existing AIV system such as the Telescope Simulator (through which the calibration source beams should go).

- *Physical size:*
The FTS envelope box (i.e. including all the internal components such as source, optics in longest OPD position and mechanisms) shall be no larger than 800mm x 700mm x H, see plan view sketch of the calibration cryolab below. The height H of the external envelope box is unconstrained.

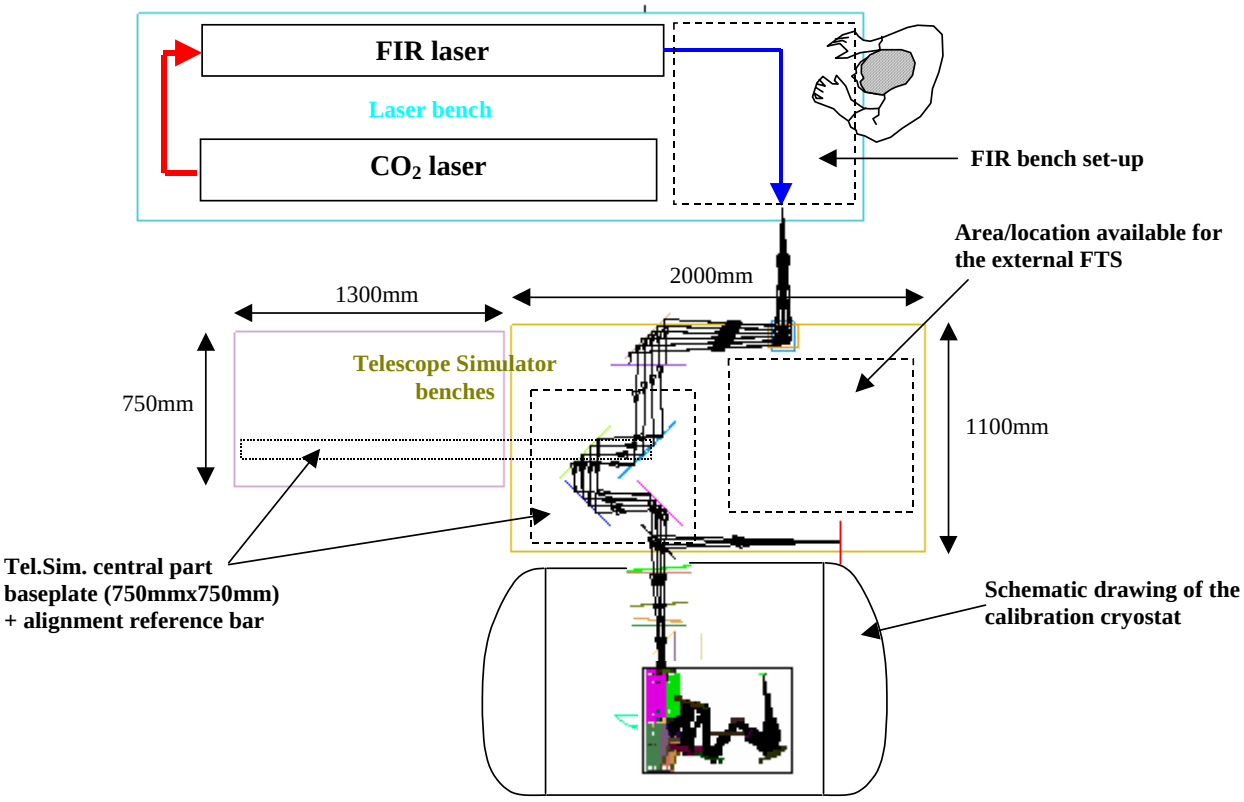

-General Interfaces:
The main Tel. Sim. bench, on which the AIV FTS is thought to seat, has a M6 holes pattern (25mm spacing), starting at 50mm from the bench edges.

The height (top surface) of the Tel.Sim. bench is ~610mm with respect to cryolab floor. The height of Herschel reference axis wrt to SPIRE in the calibration cryostat is ~850mm (see cryostat design drawing in Appendix).

The max weight of the AIV FTS could be limited to ~100kg (TBD), including its baseplate with all components on it, for practical handling reason. For comparison, the Tel.Sim. central part (mirrors, mounts, mechanisms and baseplate) is ~50kg.

The cyolab will be under dry air environment and there are no special vacuum-type specifications for the components.

- *Optical interface:*
The Tel.Sim. is based on a 1:1 point source imaging. For this reason, the FTS should deliver a point source as input to the Tel.Sim. with the following characteristics (see figure below):

- focal ratio: the AIV FTS output f-number should match the expected Tel. Sim. input of 8.68. The actual f-number is defined by the Tel.Sim. entrance pupil size and position. In practice, F~8.0-8.5 are OK as slight over-illumination of the pupil mask can be controlled.

- aperture: the filed stop defining the point source aperture should be no larger than ~2Fλ in diameter, actually ~Fλ should be preferred (being linked to the wavelength, variable aperture can be used) if sufficient output power can be obtained.
- positioning: the height of the FTS output beam should be ~240mm above the Tel.Sim. bench surface. Height adjustment (over ±10mm min., TBD) should be developed to handle the potential environmental effects (weight of cryostat locally changing the floor reference, SPIRE movement during warm/cold cycle, …). The mirror-to-best focus distance of the mirror M2 is 1970mm and stands as the (folded) optical path length between M2 and the FTS output point. Alignment (i.e. to realise the focus of M2) is based, as for the FIR laser input point, on visible laser beam from M2 permanent reference (on long bar) for angular alignment and white light illumination for (axial) focus retrieval.

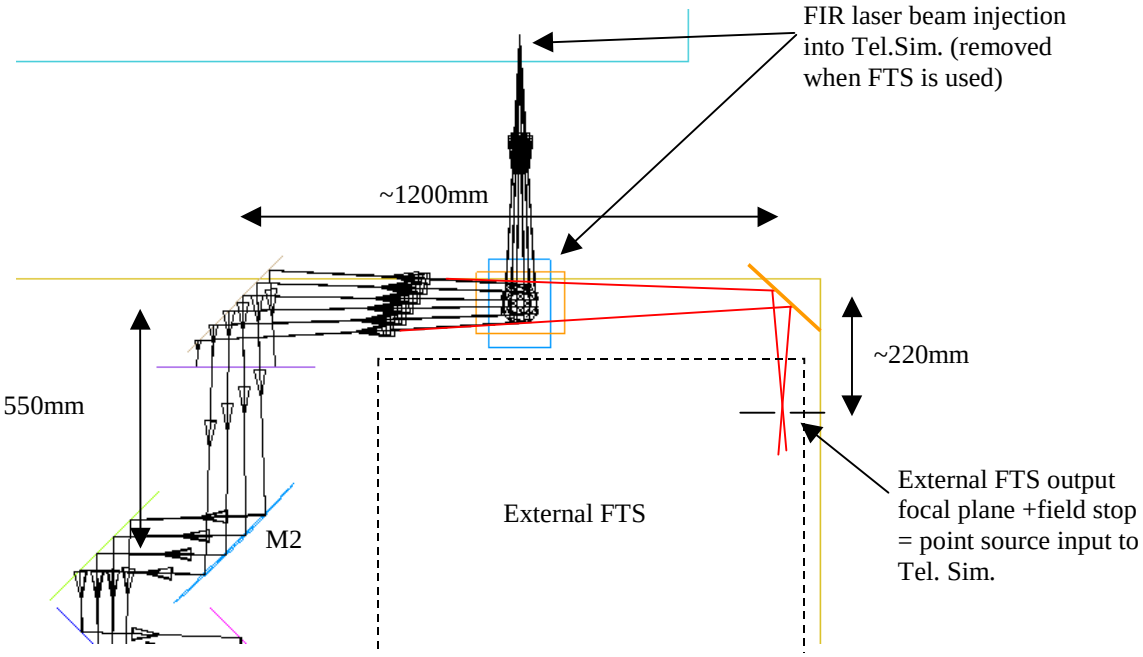

Figure 8: External FTS input into the Telescope Simulator system

- *Other:*
The FTS source could be a spectrally broad source such as blackbody or arc lamp.

The spectral resolution should be such that the SPIRE resolution can be measured and therefore can be baselined as comparable. Typical resolution of 0.1cm^{-1} (TBC) should lead to a minimum OPD of 100mm, to be included in the FTS overall design.

The mechanisms of the FTS (OPD control) should be remotely controlled from a PC under LabView (TBC) to be compliant with the TFCS and general EGSE.

3.2 Recent characterisation tests with TFTS and He-cooled Si bolometer

3.2.1 Test set-up

Test carried on 15/07/2005. The source is HBB at 1200degC. Dry air system was in used in TFTS + TelSim enclosure. Si bolometer at 4K (previously specifically purchased from QMCI Ltd), inside its dewar, with approximately tilted 100cm^{-1} filter in front was located on special table inside SPIRE cryostat, manually coarsely aligned with fine-tuning for maximum signal strength with TelSim control from TFCS. Extra cryostat filter added.
Chopper was located at TFTS output (frequency ~40Hz), with demodulation with lock-in amplifier of the signal from Si bolometer. Iris aperture at TFTS output had ~10mm hole diameter.
TFTS scans (scan mirror speed ~50μm/s and 100μ/s) piloted from SCOS. Signal from lock-in amplifier is acquired via LabView program onto TFCS for monitoring and outputting in text file (ASCII format).

3.2.2 Results

The 1st scan recorded is "scan02.txt", shown partially below, after baseline removal. Horizontal axis is time in seconds (final sampling in time)

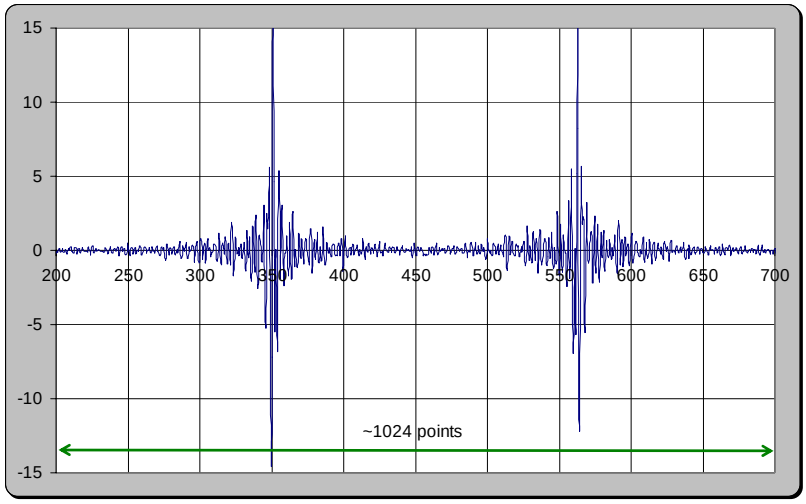

Basic manual data reduction was applied as follows: linear fit to the baseline and removal from data, extraction of central ~400points for each interferogram (forward and reverse from 1 complete scan) + zero-padding (approximately symmetric) up to 1024 points then FFT without apodisation. Spectra are then combined (averaged) and normalised. Scaling factor is applied to wavenumber axis to match (no correction i.e. assumed regular sampling in time and velocity of scan mirror) most atmospheric lines.
NB: because FT is linear, the averaging can be done before or after the Fourier transform. To avoid re-sampling of the interferograms, it was quicker and easier to average spectra. Result is displayed below.

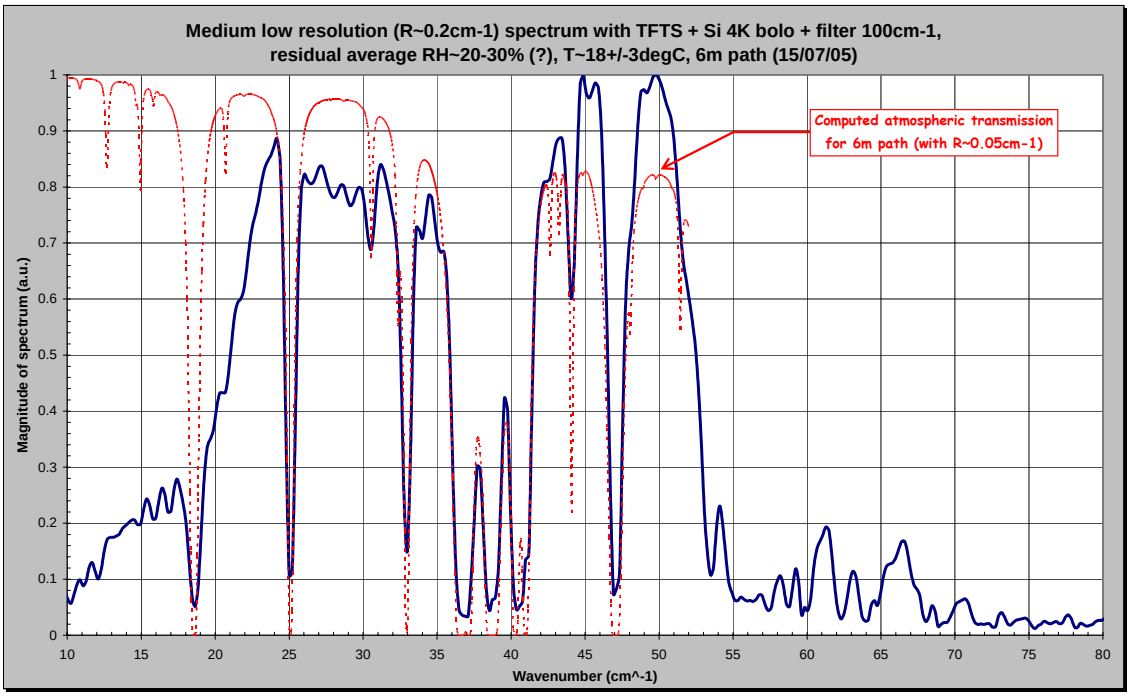

The scan sequence "scan03.txt" is shown below. 10 pairs of interferograms were acquired in ~1h45min. Over this period of time, the signal has fluctuated (relative humidity fluctuations & convection along the optical path, T stability of detector?) which forces a local linear baseline fit around each interferogram central parts or higher order polynomial fit of the baseline.

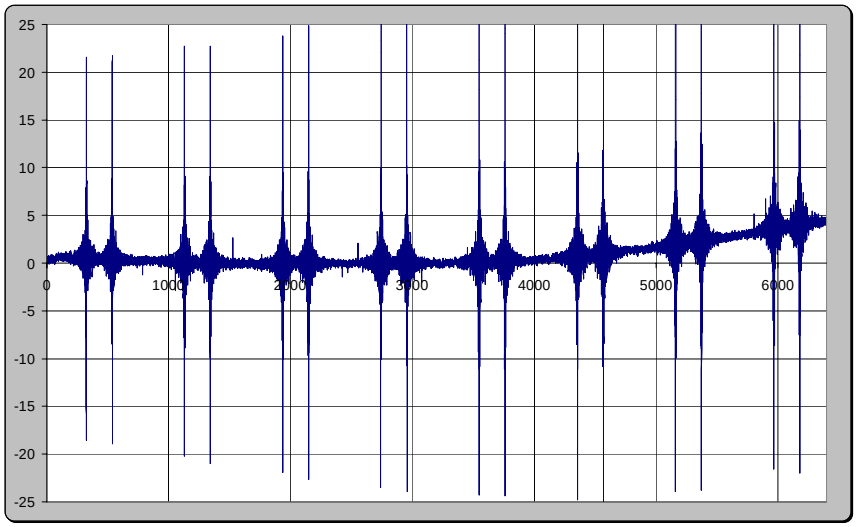

Spectrum as per "scan02.txt" above is expected (similar spectral interval and therefore resolution with 10min data around each ZPD + low level zero-padding to 2048 points) but with lower rms deviations and base noise from multiple averaging as can be seen in the plot below (averaged over spectra of the first 16 interferograms). Aging the spectrum is arbitrary normalised to the local max; this allow simpler comparison on same scale with computed atmospheric transmission.

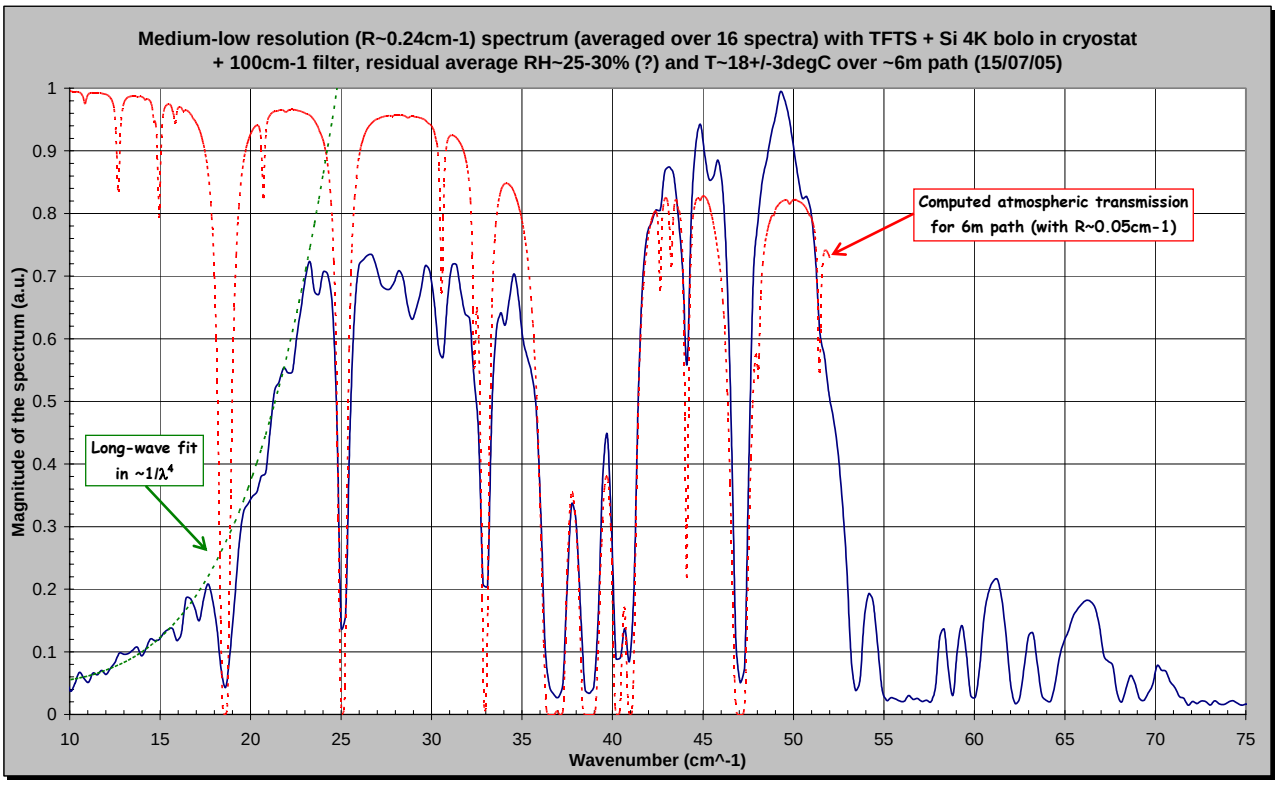

The high resolution scan "scan04.txt" lasted from more than 1h. Single forward and reverse interferogram were obtained (see plot below, after linear baseline removal) with relative overall signal stability.

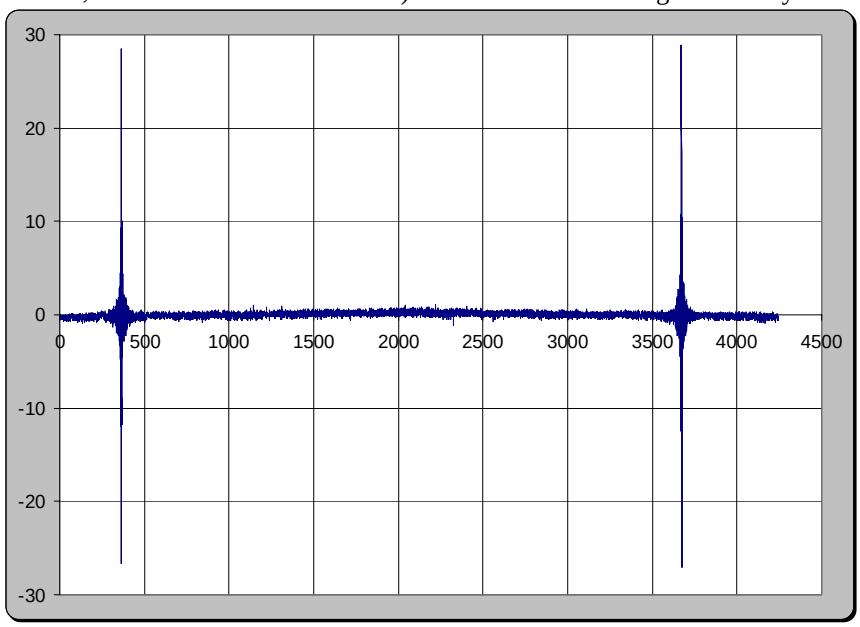

Same processing as for "scan02.txt" was applied (this time on 4096 points per interferogram) and result is shown below. The approximate spectral band extents for the previously tested SPIRE bands are also displayed in the graph.

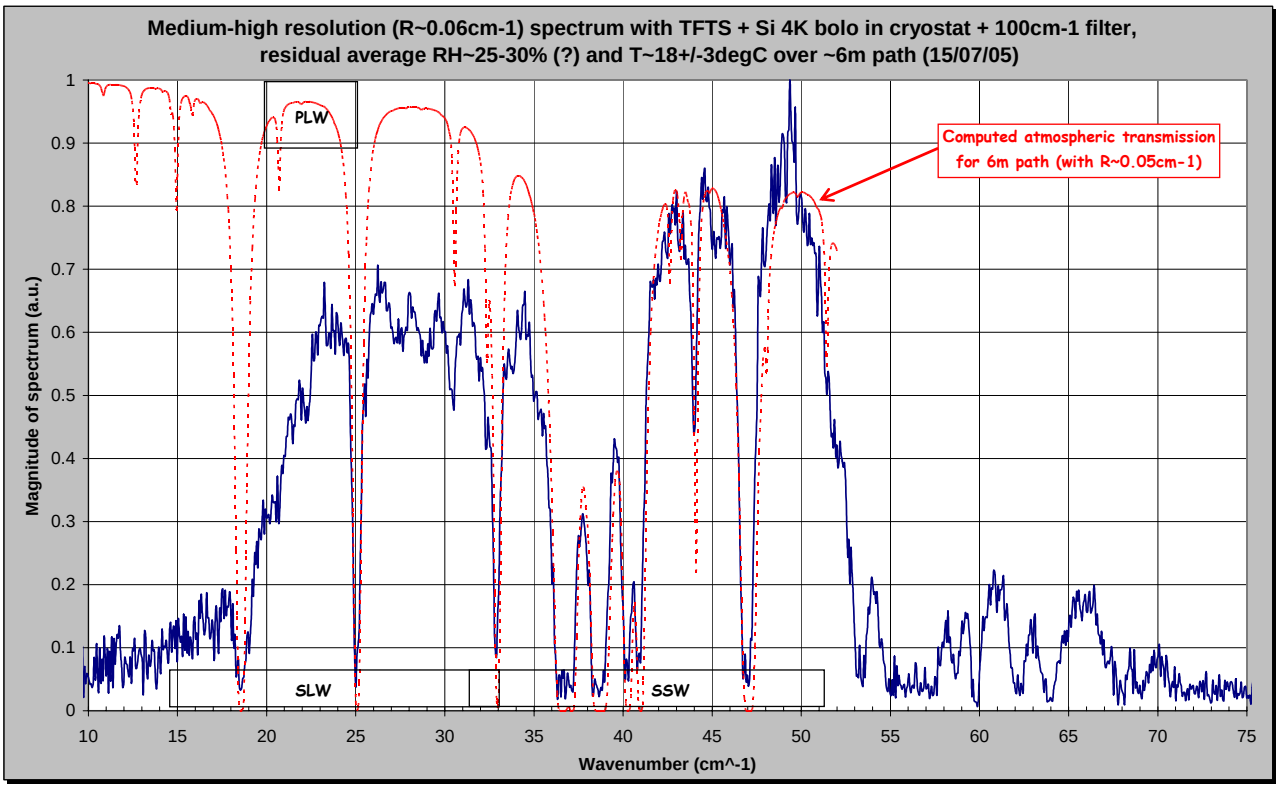

3.2.3 Some remarks regarding the derived spectra

The low and high resolution spectra are in good agreement with previous measurements (in June/July/Aug 04, see plots below for comparison) with the same source, path and detector system; most of the deep localised absorption features being identified as due to the atmosphere. Typically for wavenumber higher than ~36cm^{-1}, the measured spectrum is completely dominated by the atmospheric processes along the path.

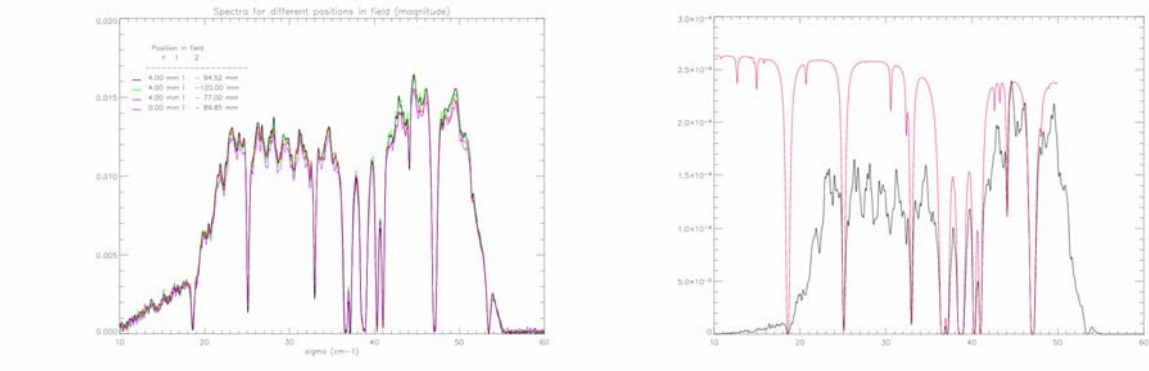

The additional filter in the cryostat filter chain does not seem to induce any major change in the spectral response. In particular the fringing with period ~2cm-1 (i.e. component separation of ~2.5mm, Si bolo dewar window and/or filter ?) most noticeable between ~25 cm^{-1} and ~33cm^{-1} is not affected/changed. Only the high resolution spectrum can give some indication about potential fringing with ~0.2-0.3cm^{-1} period corresponding to the approximate separation of the new filter with nearby component. After zooming-in, it is not obvious that such fringing appear (of it appears it is low fringing amplitude) showing that the tilt and in-band transmission of the filter are OK.

Other features to notice is the long wavelength attenuation (between 15cm^{-1} and 22cm^{-1}, approximately fitted by a ~1/λ^4 variations as see in the "scan03.txt" case result above, atmosphere removed in-band) in the spectra still present (with likely source/mechanism inside the TFTS) and will likely affect PLW measured spectral response again.
Some "leakage" (as it does not look like harmonics) between 55cm^{-1} and 75cm^{-1} could be worrying because at short wavelengths. SPIRE Phot is self-shielded from this due to single mode behaviour of the feedhorn in each band. SPIRE Spectro has to rely on good (?) short wave rejection of its own filters though in order to be sure that eventual source leakage through cryostat filters are not affecting the ground performances measurement.

3.2.4 Approximate model of the measured transmission spectrum

Based on the above, an approximate model of the measured spectrum was made; overlapping with the low resolution data from "scan03.txt" is shown below.

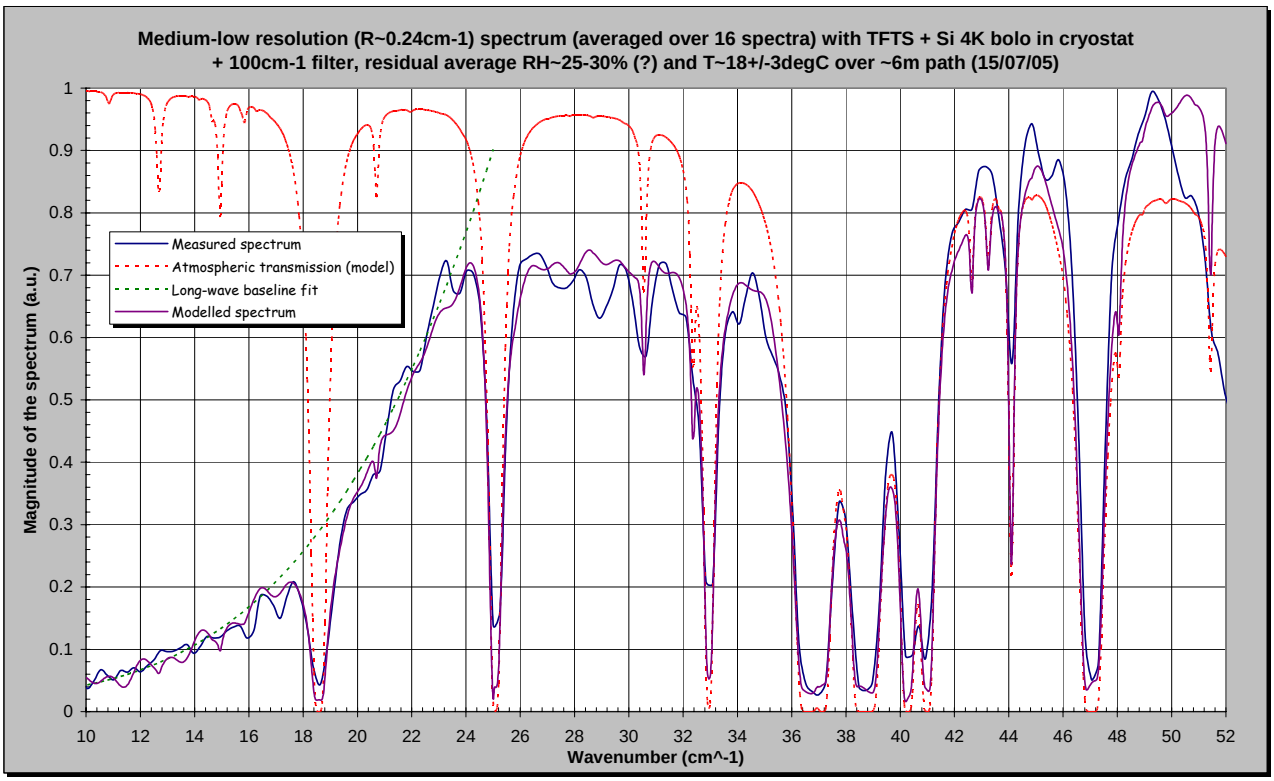

The model is base on the following:

$$S_{approx}(\sigma) = \tau(\sigma).f(\sigma) + \sum_i A_i.\cos(\frac{2\pi}{T_i}.\sigma + \varphi_i) + B$$

where τ is spectral transmission of the atmosphere along the path (previously MODTRAN computed for standard atmosphere, 6m path), *f* is attempting to take into account the spectral variations of the source spectrum (HBB in the Rayleigh-Jeans region), the detector spectral response and other effects within the system used. The term *f* is varying as 1/λ^4 up to ~25cm^{-1} and 1/λ^2 for higher wavenumber.
B is a residual noise background taken as constant and ~a few % here. The additional cosine terms attempt to handle the noticed fringing. Here, 2 cosine terms were used with amplitude of a few % and period of around ~1cm^{-1} and the slightly more dominant ~2cm^{-1} (corresponding respectively to eventual double reflection in the path with separation of ~5mm and 2.5mm respectively).Their respective phase terms was manually adjusted to approximately visually improve the matching with the measured spectrum. There are more dominant in the 24-34cm^{-1} region and seems to be well explained by the Si bolometer internal filter and window (thickness and separation) which can not be tilted as internal to the detector dewar. It is therefore not expected that this instrumental fringing will appear during use of the TFTS with SPIRE.

Good qualitative agreement is found when compared below with the medium-high resolution spectrum.

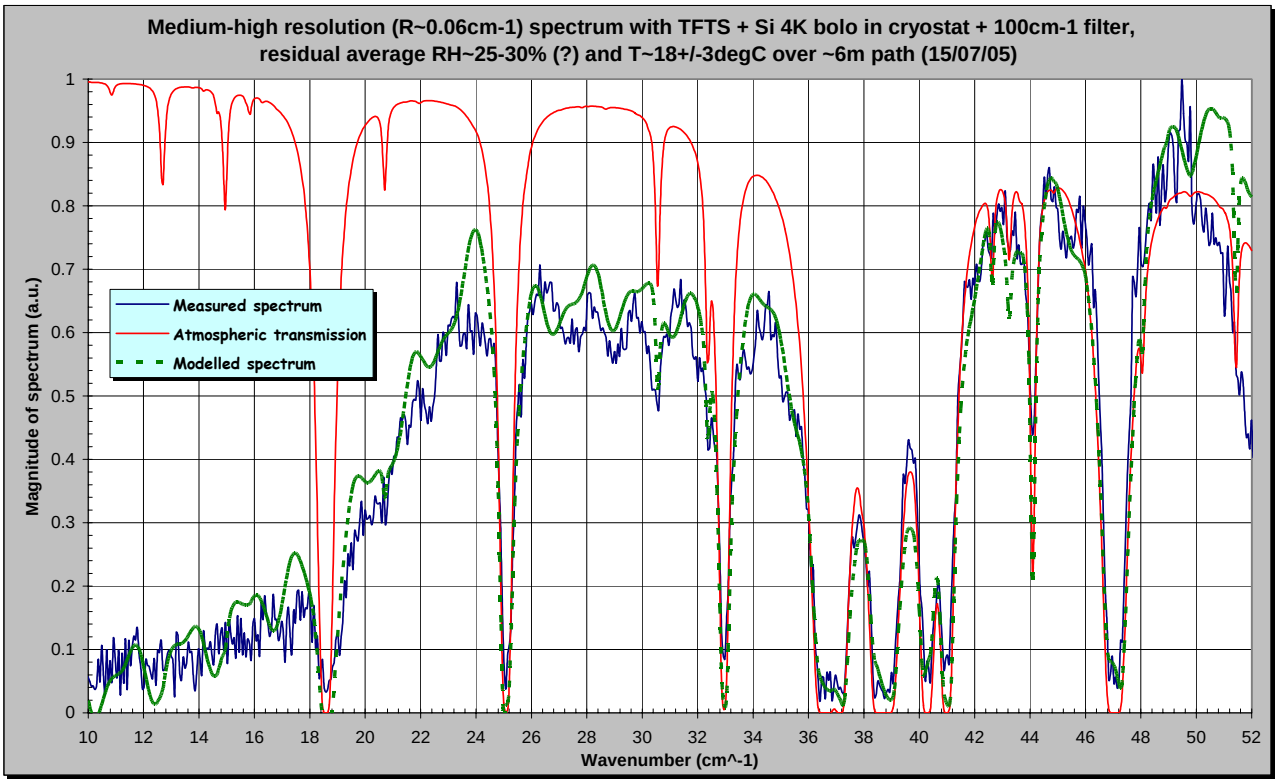

3.3 Remarks on the TFTS and proposal for related recommended actions

3.3.1 General concerns

Beginning of November 2005, we had an opportunity to use for a few hours a broadband uncooled detector array (128x128, ref. SPIRICON PYROCAM III). Although it was intended to perform further characterisation of the FIR laser beam at different wavelengths, the FIR laser in maintenance was ready to be used and then it was attempted to use to the sensor, along side 50cm^{-1} and/or 100cm^{-1} edge filters, to measure the TFTS output beam with the HBB source at the nominal 1200degC. Only the TFTS image plane iris was removed and replaced by the detecting array.

Results displayed below gives the confirmation of a large spatially broadband quasi-uniform/slowly decreasing from the centre illumination of the TFTS image plane.

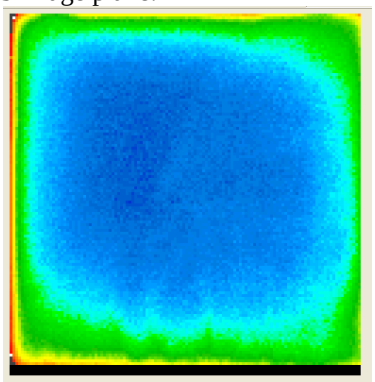

Figure 9: measured illumination at TFTS output focal plane. Inverse false colour image over full sensor array size i.e. ~12.5mm x 12.5mm.

In order to further understand it, a Zemax model of the TFTS was quickly developed, based on element separation and size taken from the built TFTS.
Simulations (see below) of the output image plane geometric illumination indicate as expected a similar behaviour if at the input plane an extended uniform source (size 10mm diameter, taken from ISOTECH Pegasus R Model 970 datasheet) is implemented. Best results based on qualitative agreement with the measurement above are found if the extended source is axially displaced by ~+ or -25mm from the TFTS optics geometric input focal plane (verification of the nominal non-confocality of the HBB planar emitting source and the TFTS optics at that location will be done; NB: due to the design of the HBB cavity, it is possible that there is a difference between the physical HBB emitting plane and the effective/apparent emitting surface coupled to the TFTS optics).

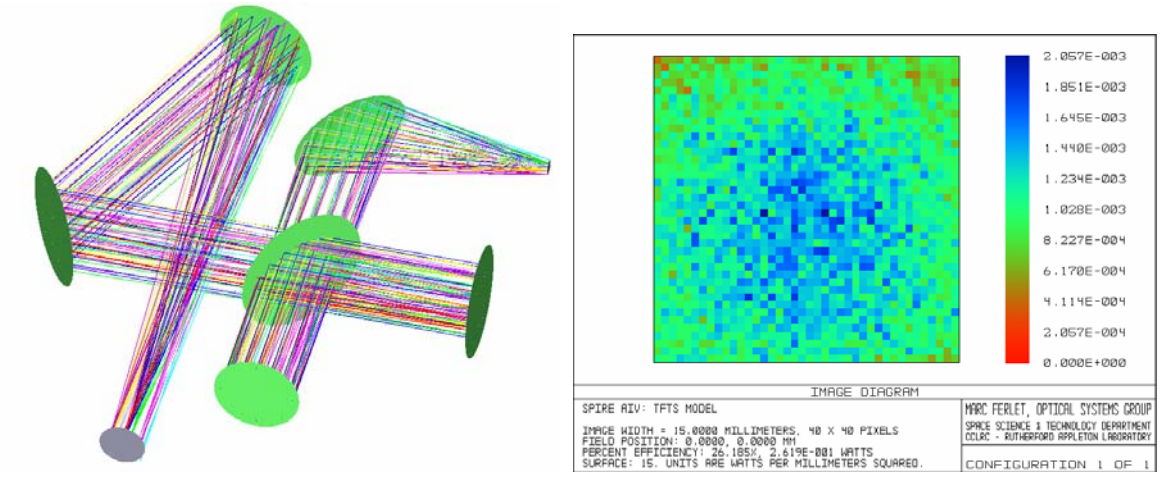

Figure 10: Layout from TFTS model (BS is inverted on the drawing due to simple sequential implementation of the model) (left) and output computed illumination (>10^5 rays) over 15mmx15mm with 25mm defocus at input focal plane of a 10 mm diameter extended source, assumed on-axis (right).

More quantitatively, one can consider a PLW pixel as receiver. Its apparent size at the SPIRE entrance focal plane (= same at TFTS output as TelSim is doing 1:1 imaging) would be ~5*(8.7/5)~8.7mm diameter. Assuming a slight oversize of the TFTS output iris to avoid being dominant while maintaining power into a single re-imaged pixel, one can estimate the amount of power (via relative encircled energy falling into this pixel) for different size of the TFTS on-axis extended source object. This is summarised in the plot below, after taking into account the geometry of the uniformly bright source and the TFTS (i.e. extended field only imaged perfectly on-axis otherwise aberrated, de-magnification factor from the TFTS optical design, residual vignetting/spillover, …) and diffractive effect averaged over PLW spectral range (assumed spectrally flat here).

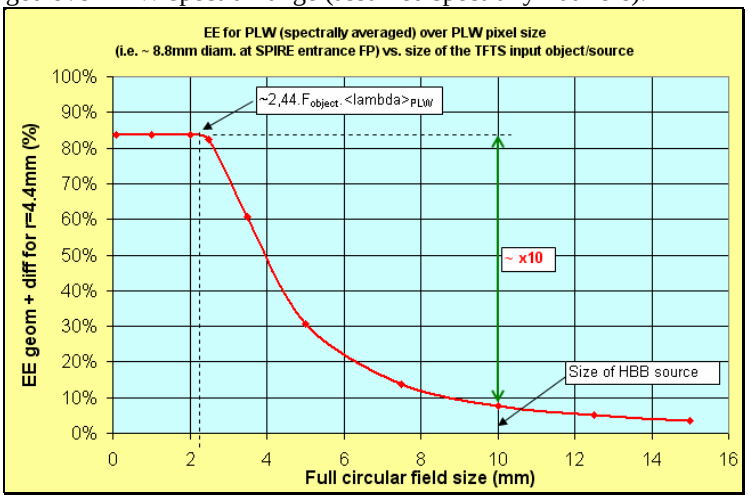

Figure 11: Use of the TFTS model to estimate the PLW in-band power falling into 1 pixel as function of the size of the input source.

There are mainly 2 interesting things to notice:

1- Below about 2.2mm diameter, the coupling (at least in term of EE) is quasi maximal in theory which is expected because the source extent becomes smaller than the in-band averaged Airy disc size and therefore the object plane illumination is quasi-equivalent to a point source (and so coupling in theory up to ~84% into a 2.4Fλ sized receiver aperture);
2- The actual HBB source extent is 10mm diameter and because of the spatial "dilution" of power (from extended field aberrations, demagnification, diffraction) at the TFTS output plane, we are coupling only ~1/10th of the maximal possible, even with quite open output iris.

This behaviour is similar in the other SPIRE bands. In summary, we can say that in theory a factor x10±2 in the amount of power from the HBB towards any SPIRE pixel could be gained. In practice, we could more reasonably expect between x2 and x5-6 TBC at best. This may not be negligible for SPIRE as it could potentially improve accordingly the SNR for spatial and spectral tests with broadband quasi-point sources.

Also one can wonder if the limitations due to the finite extent of the iris aperture at the TFTS output is not preventing some of the source radiation (typically longer part of the spectrum) to be coupled to the TelSim and be re-imaged towards SPIRE. For that, the same EE computations are performed but this time as function of λ for a typical given size of output iris aperture (taken as 3.2mm diameter as per a lot of PFM2 performances tests; in order to be smaller than even PSW pixel image while still allowing for a certain amount flux to reach the SPIRE). Results are shown below for the case of PLW spectral range, along is plotted a low resolution TFTS spectrum measured with 4K Si-bolometer before PFM2 test campaign (July05, see previous note). One can notice that this effect is not enough to explain the decrease at long wavelength over PLW range. More, if the computations are repeated for larger iris aperture the slope is less pronounced while last year experiments showed that the impact of the iris aperture diameter was small on the spectrum shape in the region. This tends to indicate that other mechanism(s) (potentially such as λ-dependent TFTS internal vignetting & spillover, λ-dependent emissivity and/or thickness of the HBB emitting source, BS response ?, …) are still needed to explain it fully. Nevertheless the availability of experimental spectra taken with and without SPIRE can allow retrieval of the SPIRE only spectral response per bands including PLW so this is not crucial for SPIRE ground calibration.

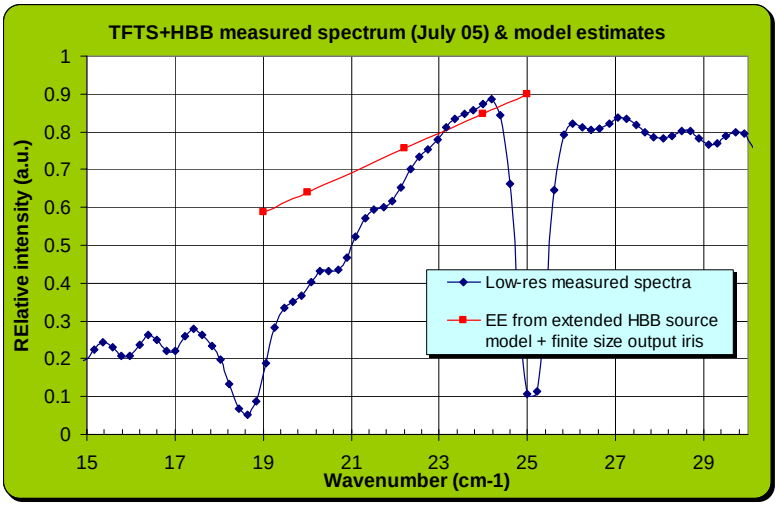

Figure 12: Computed EE for 10mm diameter HBB source and 3.2mm diameter iris aperture in the PLW band compared to some recently measured TFTS spectrum.

3.3.2 Practical considerations for potential improvement

The goal is to recover the largest part possible of presently uncoupled power from the HBB source without the minimal amount of modifications to the TFTS present configuration and interfaces. A proposed plan with 3 steps increasing in relative complexity and impact (while attempting to remain well within the limitations of the previous sentence) is given below. It is suggested that for each step an experimental verification based on broadband spectra acquisition with the TFTS is performed. They can be used as reference for comparison of the

effectiveness of the modifications while becoming as well, in case of acceptance of the modification (best results), the reference Test facility instrumentation characterisation spectra before PFM3 test campaign.

1) The HBB is defocus axially positively and negatively compared to its present location. Practical limitation due to HBB size and nearby structure (mostly enclosure walls or beams) will limit these to a few cm max TBC but this should be still larger than the in-band depth-of-field.

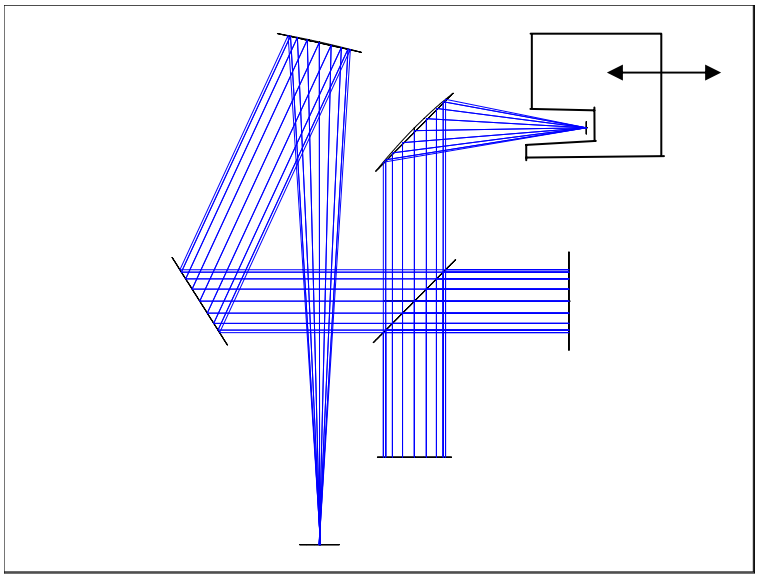

Lowest impact, easiest to implement but expectation of gain of only 10-50% TBC.

2) Turning effectively the TFTS in a more standard and simple Michelson: the first parabolic mirror is replaced by a flat mirror. The long aspect ratio HBB cavity design will emit with a relatively low divergence. The optics at the output of the [illegible] untouched to allow for the initial as per design refocusing towards output iris [illegible]er.

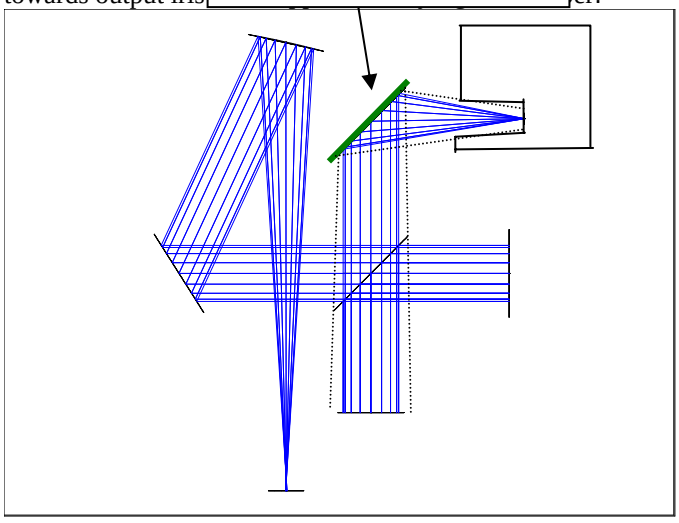

The source beam divergence inside the interferometer when the moving mirror is scanning will limit (at long wavelength) the effective resolution (but this should be acceptable here) and loss by vignetting and spillover on finite size components and aperture are to be expected. Expectation of gain may be up to ~x2 in this configuration.

3) Forcing a real point source object at the TFTS entrance focal plane:

The TFTS is untouched but the HBB is replaced by extra parabolic mirror, confocal with the present first paraboloid. The full emitting surface of the HBB is refocus onto a point source (in practice extended to several mm in diameter due to diffraction, but ok as along as equal or smaller than the point source range limit in fig.3) at the TFTS input focal plane and from there gets modulated by interferometer in the standard way and re-imaged as per design to the interface plane with TelSim.

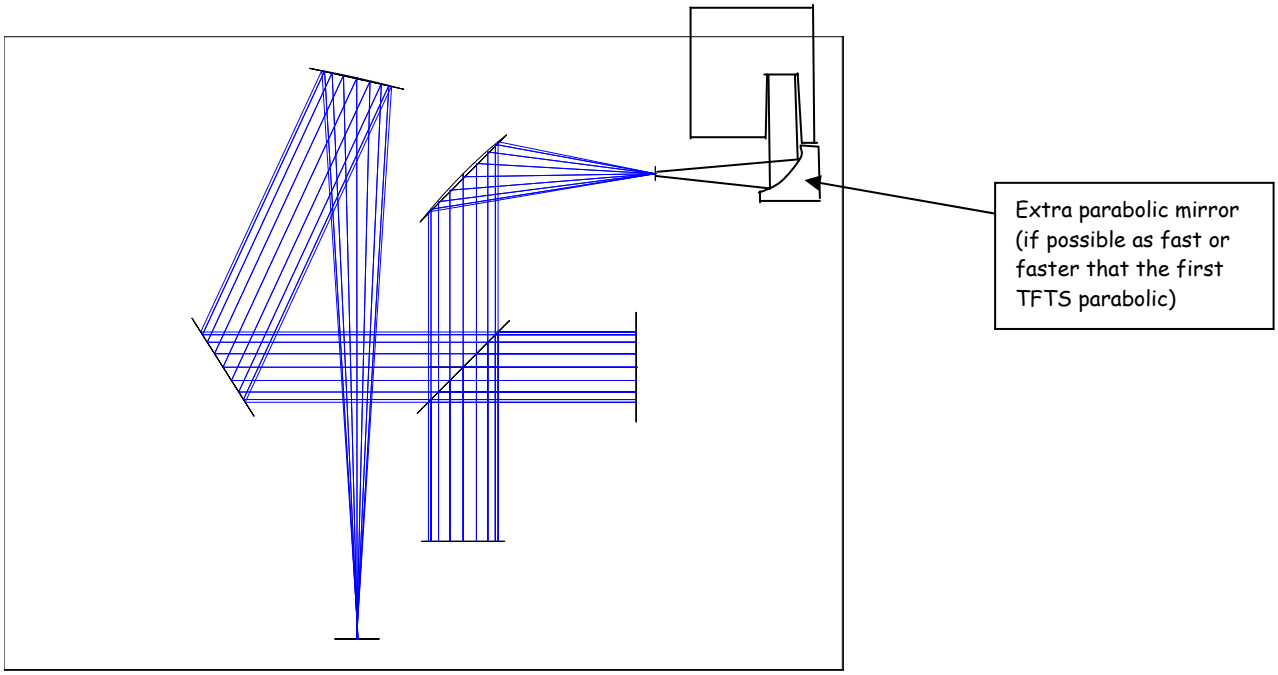

In practice, by lack of space, the HBB may be raised on a table above the plane of the TFTS and coupled to the first extra parabola via extra out-of-plane folding mirror. Potential practical gain here can be between x4 and x6 approximately.

4. PHOTOMIXING SOURCE

In complement of the FIR laser which has decreasing output power when used at longer wavelength (typically >500μm), a photomixer diode source (borrowed from and developed by RAL/SSTD MMT group for the ALMA project) was injected into TelSim via some of the FIR laser beam shaping optics (+ remote control of NIR sources before external to cleanroom lab, see pic below; the photomixing diode in the lab is fed via a long fibre optics).

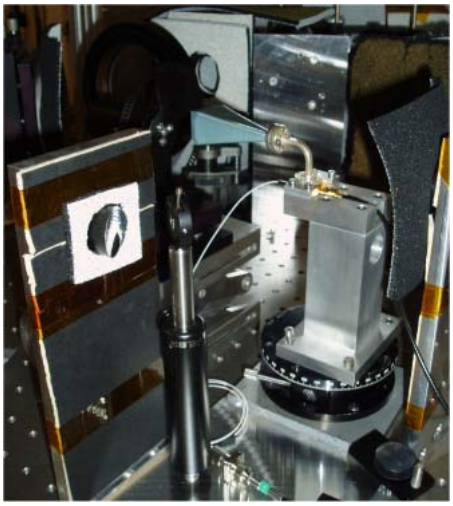

The source is expected low power so that only SPIRE is sensitive enough to detect it (Si bolometer not practical; Golay cell can hardly separate it from noise even when chopped). but tuneable in wavelengths across LW part of SPIRE spectrum (Phot and Spectro) and quite stable (some small drift in frequency with time possible).
During PFM2 test campaign in September 2005, a quick attempt to use the photomixing source with SPIRE was performed. A decent signal was detected on SPIRE PLW & many frequencies found during frequency sweep of the source up to the long-wave edge of SLW, see summary table below.

Frequency sweep with source (via T tuning, manual) and on-the-fly monitoring (on QLA) with pointing on SLW C4 (large source aperture)

Frequency (GHz)	T (deg C)	Comments
650	8.5	*Highest frequency tried*
630	9.8	
604 (drifting closer to 601)	as per previous day	*=> low-res spectrum taken with SPIRE SMEC on SLW C4*
509.5	as per previous day	*=> low-res spectrum taken with SPIRE SMEC on SLW C4*
491.5	19	
470	21	
460	25.3 ?	*Lowest fregency giving a signal on SLW (band edge ~450-430GHz)*

Remarks: All approximately equal strength as seen by SPIRE => probably more power at source for the lowest frequencies but filtered/vignetted at injection into TelSim
More frequencies but the one found previously between 500 and 600GHz are not reported because as per previous day
Signal strenght lower than for PLW test the previous day for same SPIRE pixel size => due to extra BS in Spectro chain, not perfectly on white fringe, larger bandpass than PLW

A few source spectra were taken via low-res SMEC scans on SPIRE SLW (TelSim pointing on SLW pixel C4); results processed by Locke Spencer (Uni. Of Lethebridge) and presented at SPIRE SDAG meeting in December 2005 are shown below. This confirms the low power, unresolved at low-resolution (exact variations of the source bandwidth with central wavelength is TBC) but detectable signal by SPIRE even in the case of broadband detector as for SLW receiving the full-field load from filtered room-temperature background.

- Case of frequency selected around ~601GHz:

SLW C4 – should be 20.033cm-1

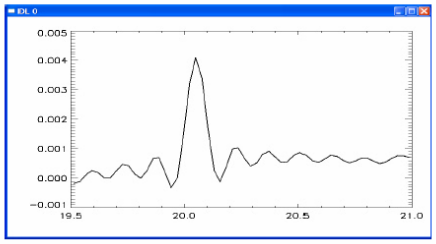

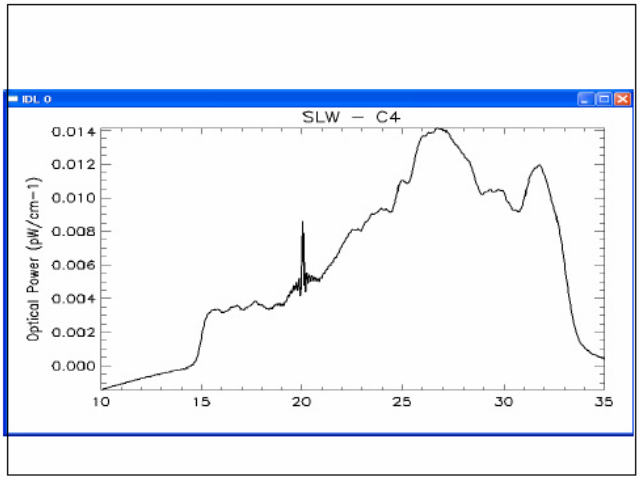

601 GHz = 20.03333 cm-1

- FWHM = 0.04007 cm-1
- Amplitude = 4.097 fW/cm-1
- Line Centre = 20.05 cm-1
  - Line centre error (2/5 δσ)
- Area = 0.1638 fW

- Case of frequency selected around ~509.5GHz:

SLW C4 – should be 16.9833cm-1

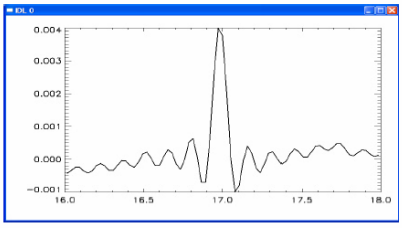

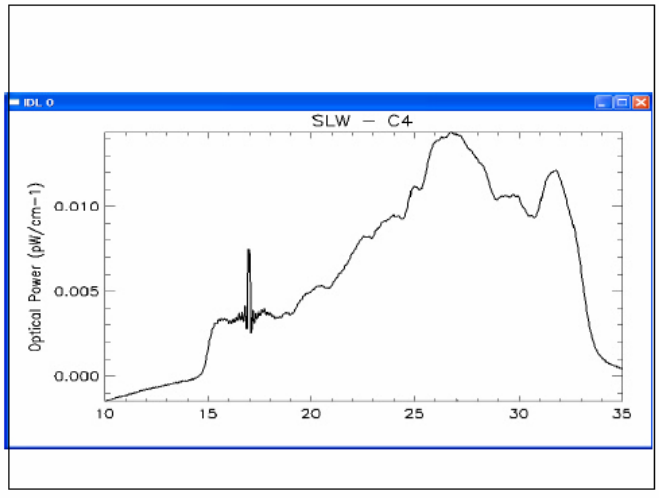

509.5 GHz = 16.983333 cm-1

- FWHM = 0.07554 cm-1
- Amplitude = 3.994 fW/ cm-1
- Line Centre = 16.981 cm-1
  - Line centre error 0.002cm-1 (1/20 δσ)
- Area = 0.3365 fW